

Experimental Study of a Flow into an Engine Cylinder Using PIV

Alessandro Davario* and Vincenzo Di Lella*
Alma Mater Studiorum, Università di Bologna, 47121 Forlì, Italy

This work is focused on the study of the tumble and the swirl motions, which develop during the intake stroke inside a cylinder of a Diesel engine. These motions are analysed by means of standard and stereoscopic Particle Image Velocimetry (PIV) techniques. Due to the incompressible characteristic of the flow involved, a steady flow test bench is used. Analysing the swirl motion, it is possible to identify three main regions along the cylinder, characterized by different vortex structures. Moreover, a coherent structure, single-vortex dominated is detected in the region distant from the valves. Regarding the tumble plane, a strong recirculation bubble is produced, even though there is no piston inside the cylinder. In addition, the velocity field into the entire cylinder volume is extracted by means of a three-dimensional three-component reconstruction. Finally, these results are compared with LES results, in order to validate the latest.

The work was performed as part of a Dual Master programme between the University of Bologna and KTH, Stockholm, between January and June 2017. The work was conducted as a collaboration between the KTH Mechanics department and the Engine Development, Gas Exchange Performance (NMGP) division at Scania CV AB, situated in Södertälje, Sweden.

I. Introduction

Nowadays, fuel consumption and emissions are a main concern for car and truck industries. A reduction of both is required, due to several aspects. In particular, the constant rise of fuel price and the increasingly stringent regulations lead to a continuous research of new solutions to satisfy these objectives.

Emission standards are defined by a series of European Union directives. These standards target most part of the vehicles: cars, trucks, locomotives and similar machinery. Several emissions are of main interest for the environmental safeguard: nitrogen oxides (NO_x), non-methane hydrocarbons (NMHC), total hydrocarbon (THC), carbon monoxide (CO) and particulate matter (PM). With regards to Diesel engines, NO_x and PM are of main concern. In an industry with an increasing environmental awareness, Scania developed a complete package to reduce fuel consumptions in the context of an industry characterized by increasing emissions, called Ecolution. The main objective of this programme is to decrease fuel consumption by more than 10%.

To reach all these requirements, it is important to have the best combustion process. Then, understanding air and fuel motion inside a diesel engine is a key aspect. A fundamental role, during the combustion process, is played by tumble and swirl motions. Inducing these two motions, a better mixing of the fuel and air inside the combustion chamber can be achieved. For this reason, important care is taken in the design of the cylinder head.

The aim of this work is to investigate tumble and swirl motions by means of the Particle Image Velocimetry technique. For this purpose, a specific cylinder head, made available by Scania, is tested. In particular, the work is focused on the identification of the main structures contributing to swirl and tumble, induced during the intake stroke of a Diesel engine. Strong emphasis is posed on the study of their evolution. In addition, the entire velocity field inside the cylinder volume is reconstructed. Finally, the results obtained are compared with LES simulations.

This research presents a brief overview of the engine working principle and of the flow inside the cylinder in section II. In section III, first of all the PIV technique is explained, including the calibration procedure and the related issues. In addition, the instrumentation used and experimental configurations adopted are described in detail. The data obtained have been processed using different methods, presented in section IV. Finally, the results and the related conclusions are discussed in section V.

II. Theoretical Background

II.A. Fluid motion inside cylinder: tumble and swirl

Due to the specific geometry of engine valves and ports, two different types of organized motion are induced inside the cylinder. These motions have a specific direction. However, since the mean velocities are usually smaller than

*M.Sc. Aerospace Engineering candidate, alessandro.davario@studio.unibo.it, vincenzo.dilella@studio.unibo.it

turbulent velocities, these organized motions, usually referred in the literature as coherent motion, are "hidden" inside the disorganized turbulence. Therefore, in order to find the organized part and thus to have a clear visualization of it, it is necessary to have a number of measurements large enough to allow a statistical analysis and to find the average flow pattern. These two kinds of motion are related, since as swirl is generated, tumble motion is also induced. There are several reasons why it is so important to induce swirl and tumble inside the cylinder. The most important reason is to provide high turbulence levels at ignition. Indeed, this fact will result in higher flame speeds, thus leading to a more efficient combustion process. In addition, another fundamental aspect lies on the energy content. Indeed, the free turbulence is more dissipative than an organized motion, which will result in a rapid decay of the energy in the inlet jet. However, the basic idea of such motions is to try to retain some of the momentum of the inlet jet, in order to have high energetic levels for a longer period.

Another important aspect to underline is an interesting difference between tumble and swirl. Indeed, as the piston reaches the top dead centre, the tumble always breaks down to turbulence, since there is not enough space to contain a vortex of such dimensions. The same does not happen for the swirl, in case of particular combustion chamber shapes, as reported in [1]. Therefore, swirl does not break up into turbulence and this will result in a good way to control the combustion process and the flame propagation.

II.B. Incompressible Navier-Stokes equations

Due to the state of the fluid involved in this study, an important assumption can be done. Indeed, since only the intake stroke is taken into consideration, it is reasonable to assume an incompressible flow (Mach number $M < 0.3$), in which variations of density due to its motion may be neglected. In particular, it is assumed that temperature fluctuations in the test rig are negligible. This important assumption leads to the so called Incompressible Navier-Stokes equations:

- Mass conservation

$$\frac{\partial u_i}{\partial x_i} = 0 \quad (1)$$

- Momentum

$$\rho \left(\frac{\partial u_i}{\partial t} + u_j \frac{\partial u_i}{\partial x_j} \right) = -\frac{\partial p}{\partial x_i} + \mu \frac{\partial^2 u_i}{\partial x_j \partial x_j} \quad (2)$$

II.C. Proper Orthogonal Decomposition: POD

Proper orthogonal decomposition is a useful method to reduce high dimensional processes representing them with few basis modes, which are able to capture the dominant components of the process considered, without losing too much information [2].

In the present study, dealing with a finite number of data, a discrete version of POD analysis is used. This analysis is referred in literature as Principal Component Analysis (PCA). In PCA the goal is to reduce the dimension of a set of correlated variables, without losing so much information regarding variation in the original data set. So, a new uncorrelated set of variables is found, called Principal Components (PCs), ordered in such a way that the first keeps most of the variation presented in the original data set. Then, keeping only the first few PCs the original space of variables can be represented, reducing its dimension, without losing too much accuracy. The aim is to find orthogonal *directions* in N -dimensional space, ordered in such a way that the first i orthogonal directions give the best possible *i-component* approximation.

To construct the POD basis different approaches exist [2]. For this study, the Singular Value Decomposition (SVD) approach is used since it can be applied also to non-square matrices.

Given any real $N \times M$ matrix \mathbf{U} , there exist orthogonal matrices, $N \times N$ \mathbf{V}^1 and $M \times M$ \mathbf{V}^2 , such that

$$(\mathbf{V}^1)^T \mathbf{U} \mathbf{V}^2 = \mathbf{S} \quad (3)$$

where \mathbf{S} is a $N \times M$ matrix with all element equal to zero, except for the main diagonal, in which these are equal to

$$s_{ii} = \sigma_i, \quad \sigma_1 > \sigma_2 > \dots > \sigma_r, \quad r = \min(M, N) \quad (4)$$

where σ_i are the singular values of the matrix \mathbf{U} , columns of \mathbf{V}^1 are the left singular vectors, and columns of \mathbf{V}^2 are the right singular vectors. A non negative σ is called singular value of the matrix \mathbf{U} if and only if there exist a unit-length N -dimensional vector \mathbf{v}^1 , and a unit-length M -dimensional vector \mathbf{v}^2 , such that

$$\mathbf{U} \mathbf{v}^2 = \sigma \mathbf{v}^1 \quad \text{and} \quad \mathbf{U}^T \mathbf{v}^1 = \sigma \mathbf{v}^2 \quad (5)$$

The number of non-zero singular values gives the rank of the matrix \mathbf{U} .

Equation (3) can be written as

$$\mathbf{U} = \mathbf{V}^1 \mathbf{S} (\mathbf{V}^2)^T \quad (6)$$

In order to obtain a matrix with a lower rank to approximate \mathbf{U} , it is possible to take only the first \mathbf{K} singular values into a square $K \times K$ diagonal matrix \mathbf{S}_K , obtaining

$$\mathbf{U} \simeq \mathbf{V}_K^1 \mathbf{S}_K (\mathbf{V}_K^2)^T \quad (7)$$

where in \mathbf{V}_K^1 and \mathbf{V}_K^2 are collected respectively the first \mathbf{K} columns of matrices \mathbf{V}^1 and \mathbf{V}^2 . With this decomposition, no other matrix with a rank equal to \mathbf{K} can better approximate the matrix \mathbf{U} , in a least square sense.

Pre-multiplying Equation (3) by \mathbf{U}^T from the left, it can be shown [2] that, defining $\mathbf{D} = \mathbf{U}^T \mathbf{U}$, and $\mathbf{S}^2 = \mathbf{S}^T \mathbf{S}$,

$$\mathbf{D} \mathbf{V}^2 = \mathbf{V}^2 \mathbf{S}^2 \quad (8)$$

where the columns of \mathbf{V}^2 are eigenvectors of matrix \mathbf{D} (modified correlation matrix), and the square roots of eigenvalues of matrix \mathbf{D} are singular values of matrix \mathbf{U} .

Similarly, pre-multiplying Equation (3) by \mathbf{U}^T from the right, it can be shown that the columns of \mathbf{V}^1 are eigenvectors of matrix $\mathbf{C} = \mathbf{U} \mathbf{U}^T$.

Based on the theoretical background explained, a MATLAB code [3] is used to perform a POD decomposition.

III. Experimental Method, Setup

To study the flow motion inside the cylinder the Particle Image Velocimetry (PIV) technique is used. It consists in different subsystems, which work harmonically to obtain good measurement results. A **Laser** is needed to illuminate the area of interest. In this work a level 4 solid-state *Neodym-YAG laser* is used, which has a wavelength of 532 nm, and a maximum light pulse of 200 mJ. Laser light is directed using **mirrors**. Flow characteristics are studied capturing the added **particle** movements with an **optics-camera**. Two CCD (Charged Coupled Device) sensors are used, each one with a resolution of 2048 x 2048 pixels, a dynamic range of 14 bits, and a maximum sampling frequency of 14 Hz. The lens used is a *Nikon 85 mm f/1.8*.

The PIV technique is chosen since it is a non-intrusive method and a whole field technique. Despite these advantages, during measurements one must remember that PIV is an indirect velocity measurement by means of added tracker particles. Particles should be small enough to follow the flow motion accurately, but big enough to allow a good light scattering. Since measurements are performed in air, a good diameter for the particles is $1 \sim 5 \mu m$ [4]. It is possible to achieve this by using a fog machine, which works with a mix of food propylene glycol and de-mineralised water. The mix has the tendency to deposit on the glass cylinder surface, leading to blurred images, in stereo-configuration. Then, a cleaning period of the glass is required.

Concerning the light source, the laser pulse should be as short as possible to avoid blurred images and long enough to accurately determine the tracker displacement. Changing measurement configuration, and measurement plane position, the optimal Δt will change. For this purpose a Δt -optimizer tool is used. The optimizer is implemented in the software which manages the entire PIV instrumentation: *DaVis* software [5]. Finally, since a high energetic laser is used, laser reflection must be avoided. Indeed, a direct exposition of the CCD sensor to the light source lead to an inevitably damage of it.

III.A. Mathematical background

Images acquired during PIV measurements are divided in interrogation areas. Taking into account one frame we can visualize a random distribution of particles. These are distributed inside the flow as $\mathbf{\Gamma} = (\mathbf{X}_1, \mathbf{X}_2, \dots, \mathbf{X}_N)$, where $\mathbf{X}_i = (X_i, Y_i, Z_i)$. Assuming a Gaussian point spread function of the imaging lens $\tau(\mathbf{x})$, in x and y , and using the Dirac delta-function shifted to position \mathbf{x}_i , the image intensity field of one exposure is given by:

$$I(\mathbf{x}, \mathbf{\Gamma}) = \sum_{i=1}^N V_0(\mathbf{X}_i) \tau(\mathbf{x} - \mathbf{x}_i) \quad (9)$$

where $V_0(\mathbf{X}_i)$ is the transfer function relating the light energy of the image of each particle i , inside the interrogation volume V_I , and the conversion in an electronic signal.

Displacement of the particles is evaluated using cross-correlation of two singly-exposed images. Indicating with D the distance covered by the particles, after some algebraic calculations [4] and [6], the equation representing the cross-correlation is:

$$R(\mathbf{x}, \mathbf{\Gamma}, \mathbf{D}) = R_C(\mathbf{x}, \mathbf{\Gamma}, \mathbf{D}) R_F(\mathbf{x}, \mathbf{\Gamma}, \mathbf{D}) + R_D(\mathbf{x}, \mathbf{\Gamma}, \mathbf{D}) \quad (10)$$

where R_C is the convolution of the average intensities, R_F is the noise component and R_D represents the particle displacement, expressed as the correlation of images of particles obtained from the first exposure, with images of the same particles obtained from the second exposure.

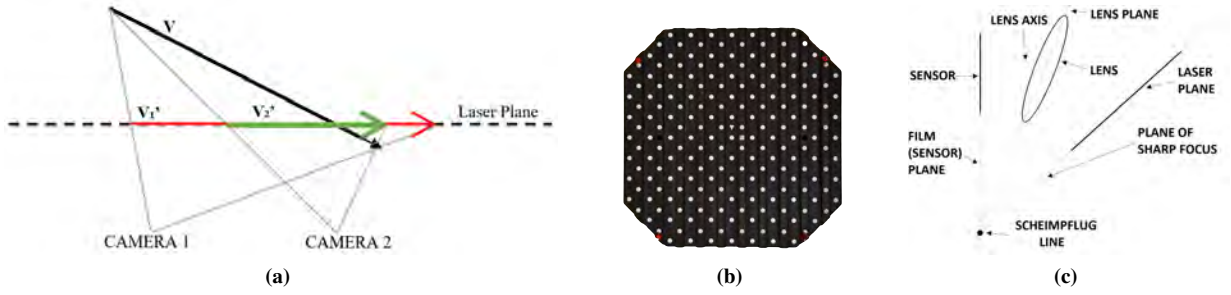


Figure 1: (a) Schematic representation of third velocity component reconstruction; (b) two level calibration plate; (c) schematic representation of the Scheimpflug rule.

III.B. Stereoscopic PIV

One of the main problems of the PIV technique is to switch from a 2D flow visualization to a 3D visualization. To extract the third component of the velocity field from a plane of the flow, a *Stereoscopic 2D-3C* method is implemented [6], using *DaVis* software. The working principle is shown in Figure 1(a): both cameras see a projection on the laser plane of the velocity vector v : v_1' is the projection for the first camera, and v_2' is the one for the second camera, using them it is possible to reconstruct the out-of-plane component.

III.C. Measurement configurations

The cylinder head is tested in two different configurations:

Mono-configuration to investigate the swirl motion. In Figure 2(a), the setup is shown. Here, the laser sheet is directly delivered to the investigation plane, and one camera is focused on the lightened zone through a mirror. The swirl motion is investigated at different distances between the cylinder head and the measurement plane (orthogonal to the cylinder axis): 42, 60, 80, 100, 120, 140, 170, 228, 300, 350 mm. For each plane, valve lifts of 10 mm and 15 mm are investigated.

Stereo-configuration to investigate the tumble motion. In Figures 2(b) and 2(c), the schematic setup is shown. Additionally, in Figure 3 the entire apparatus is reported. Here, the two cameras are pointed directly to the investigation plane, and the laser is pointed to a mirror to light up the zone of interest. Since the camera cannot cover the entire tumble motion, two planes parallel to the cylinder axis are chosen, one region close to the cylinder head (**Plane 1**), the other region positioned more downstream (**Plane 2**). A schematic representation of the plane position is shown in Figure 2(d): T_1 is the distance between the cylinder head and the starting point of the stereo measurement plane, 33 mm for Plane 1 and 112 mm for Plane 2; T_s is the stereo measurement plane length, 130 mm for Plane 1 and 141 mm for Plane 2. To investigate the entire volume, by means of a 3D3C reconstruction (see section IV.B), the position of cameras and laser is kept fixed and the cylinder head is rotated to get 36 measurement planes with 10° between each other. Each measurement is performed with a valve lift of 15 mm.

Experimental parameters are the same for each measurement: **room temperature** of 295 K; **pressure drop** inside the cylinder of 100 mmH₂O (~ 784 Pa); **air density** of 1.195 kg/m³, calculated as an average of the air density obtained using the atmospheric pressure and the air density determined with a pressure equal to $p_{atm} - \Delta p$.

For each case, 1000 snapshots are captured. The acquisition frequency is set to 7.27 Hz. However, due to the high number of snapshots the frequency is not constant during the acquisition, and it tends to increase increasing the acquisition time, due to an insufficient RAM. However, this is not a considerable issue, since the main interest is related to the mean flow characteristics.

III.D. Calibration

A fundamental step to obtain accurate results is the calibration procedure. It consists in knowing, for each camera, the viewing direction and the magnification factor. This means finding the relation between image (x,y) and object plane (X,Y) . The *DaVis* software uses an empirical calibration method,

$$\begin{aligned} X &= a_0 + a_1x + a_2y + a_3x^2 + a_4xy + a_5y^2 + \dots \\ Y &= b_0 + b_1x + b_2y + b_3x^2 + b_4xy + b_5y^2 + \dots \end{aligned} \quad (11)$$

Given reference points, the 20 unknowns are determined using a least squares approach. The image-object point pairs are extracted from a planar calibration target, which is placed coinciding with the laser sheet (Figure 1(b)).

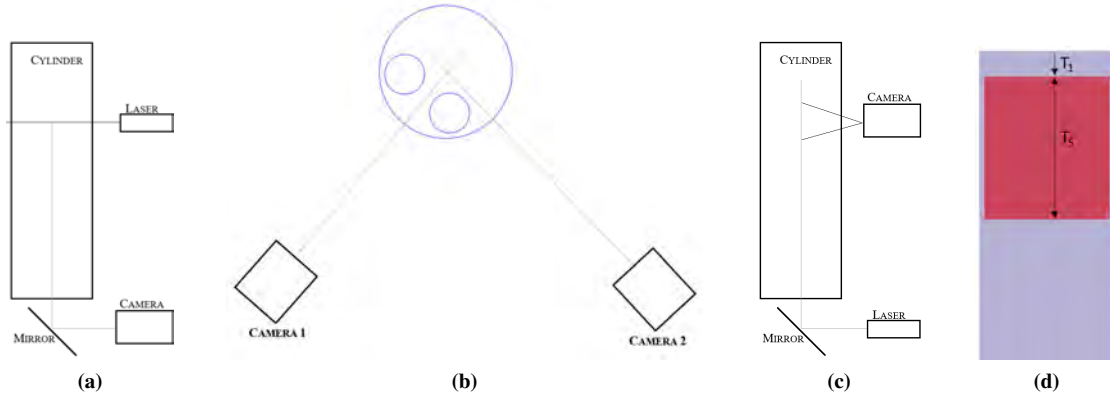


Figure 2: (a) mono-configuration; stereo-configuration (b) top and (c) lateral view; (d) stereo-plane position.

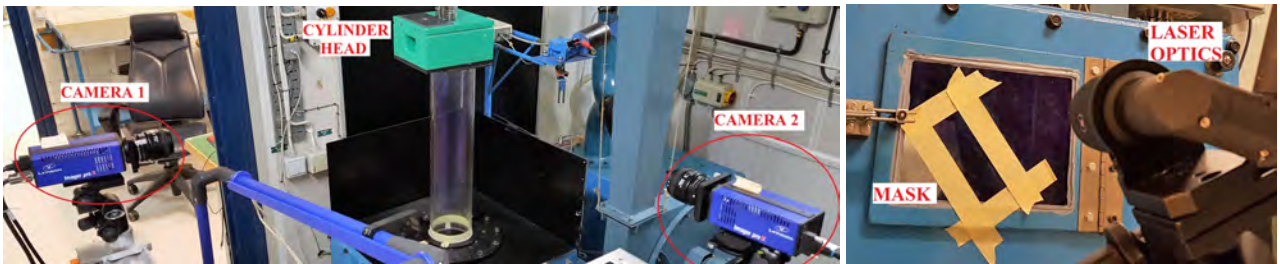


Figure 3: Stereo configuration setup. From left to right: camera positions and laser optics position.

For the mono case a **camera calibration** is sufficient. For the **stereo configuration** two non-aligned camera are used, then it is necessary to satisfy the Scheimpflug rule [7] (using a Scheimpflug adapter): *to obtain a sharp image, it is necessary that sensor plane, lens plane and plane of the sharp focus must intersect along a common line in space, Scheimpflug line* (Figure 1(c)). The final step for the stereo case is to combine the two images to obtain the third velocity component, and translate everything into the global reference system. This is done automatically by the software, which takes into account also the distortion induced by a non-orthogonal position between the camera and the measurement plane.

IV. Post-processing techniques

IV.A. Mean quantities and streamlines

The company which produces the instrumentations for PIV techniques, provides also a software to obtain the velocity vector field from PIV measurements. The raw data are used to visualize the main flow characteristics. In order to have a first understanding of the flow taken into exam, the magnitude of the average vector field V_{magn} is calculated according to the following equation:

$$V_{magn} = \sqrt{U^2 + V^2 + W^2} \quad (12)$$

where U , V and W are the three components of the average vector field. For the mono PIV configuration W is unknown, hence set to zero.

Additionally, streamlines are taken into exam to visualize the flow. They are defined as the curves that, at a given instant of time, are tangent to the velocity vectors. This definition is referred to a given time, so streamlines change in time. However, for a steady motion they remain the same, coinciding with the particle paths. In this work, a 2D streamline helps to directly visualize the presence of swirling motions or recirculation bubbles.

IV.B. Three-Dimensional Three-Component Reconstruction

One of the main objectives of this work is the reconstruction of the entire three-dimensional velocity field inside the cylinder, to find an alternative experimental way to obtain the flow structure topology. Several advanced methods, based on PIV technique, are reported in literature [9], [10].

Here a different method is adopted, and it is based on the work by Rabault [11]. As said, using a stereo PIV configuration is possible to obtain information about the 2D3C velocity field. Then, to obtain a 3D3C (three-dimensional three-component) reconstruction, keeping fixed the stereo-PIV setup, the cylinder head is rotated, with steps of 10° . In this way, the same physical plane is analysed in the entire cylinder volume. Moreover, keeping fixed the setup a considerable reduction of time is achieved. Finally, all the data acquired are translated into a global reference system and merged using Matlab through a linear interpolation, obtaining the 3D3C velocity field.

An important aspect when performing the reconstruction is the assessment of the cylinder axis. To find it, two measurement planes, with 180° between each others, can be considered. Since the data are translated to a global reference system, the set of data will contain, in a overlap region, information from both measurement planes. Therefore, it is possible to discard the redundant information, and it is easy to find the cylinder axis, which is at the middle of overlap.

IV.C. Swirl centre detection

One of the main aspect of the swirling motion is the presence of a well defined vortex, especially in the cylinder region where the flow is developed.

To detect the swirl centre several algorithms can be found in literature [8], which are quite complex. Here, the aim is to identify the core in a flow dominated principally by a single vortex. This consideration allows to use a simpler method, which has still a good accuracy. The core of a vortex $P(x_c, y_c)$ is identified as the point which minimizes the following criterion:

$$C(x, y) = 4c(x, y) + c(x + dx, y) + c(x - dx, y) + c(x, y + dy) + c(x, y - dy) \quad (13)$$

where c is the velocity magnitude, dx and dy are small lengths which are chosen according to the set of measurement data. In this work, the value for dx and dy is a displacement equal to 4 pixels.

By means of the above algorithm, it is possible to assess how the swirl centre moves during a set of snapshots. Indeed, the velocity field is subjected to small fluctuations, leading to a continuous movement of the swirl centre from one snapshot to another. In addition, the algorithm is useful to understand how the distance between cylinder head and measurement plane affects the instantaneous swirl centre position.

V. Results and Discussion

V.A. Mean velocity field in the swirl plane

Three different measurement planes are reported in Figure 5, for 15 mm valve lifts. The point of view corresponds to an observer placed below the measurement plane. The valve position is indicated in Figure 4. In this way, it is possible to have a general understanding of the flow evolution and a complete visualization of the swirling motion through the cylinder.

The main characteristic related to the swirl evolution – as also shown in [11], [12] – is that it is possible to distinguish three regions. The first one, close to the valves, is mainly characterized by a disorganized flow motion, with the presence of several vortices. In the second region, the flow is dominated by the presence of two main vortices. Finally, moving further down along the cylinder, the flow becomes more organized and this will result in the presence of a single vortex. Obviously, the three regions are different according to the two valve lifts.

To have a clear understanding, the three regions are reported in Table 1, for both valve lifts. In particular, the main difference between the two valve lifts can be appreciated in the second region. Indeed, the reorganisation of the flow structures occurs in a smaller portion of the cylinder, which corresponds to 20 mm (for the 15 mm valve lift) compared to 90 mm (for the 10 mm valve lift). This is strictly related to a higher valve lift, which allows a better working condition of the inlet ports. Moreover, this leads to a higher velocity magnitude, especially in the third region.

V.B. Swirl centre detection

In Figure 6, two different snapshots are presented. The dominant structure is conserved, but the swirl centre is considerably changing its position. Moving from top to bottom of the cylinder and having a higher valve lift lead to a more organized flow motion. This fact affects the instantaneous swirl centre position, in particular a disorganized flow will result in a more spread distribution. In order to clearly understand the aforementioned phenomenon, two different measurement

	Region 1 [mm]	Region 2 [mm]	Region 3 [mm]
10 mm	0-80	80-170	170-end
15 mm	0-80	80-100	100-end

Table 1: Region limits for both valve lifts.

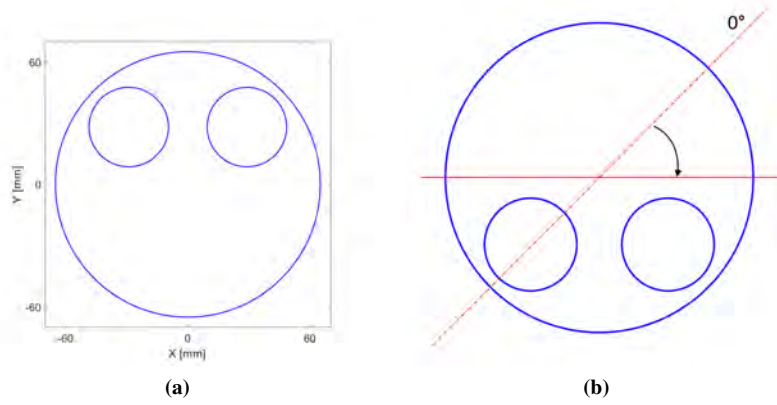


Figure 4: (a) Valve position for mono PIV configuration measurements, point of view from the bottom; (b) positive direction of rotation of the measurement plane in stereo configuration, point of view from the top. The red dashed line represents the 0° measurement plane, the arrow identifies the positive direction.

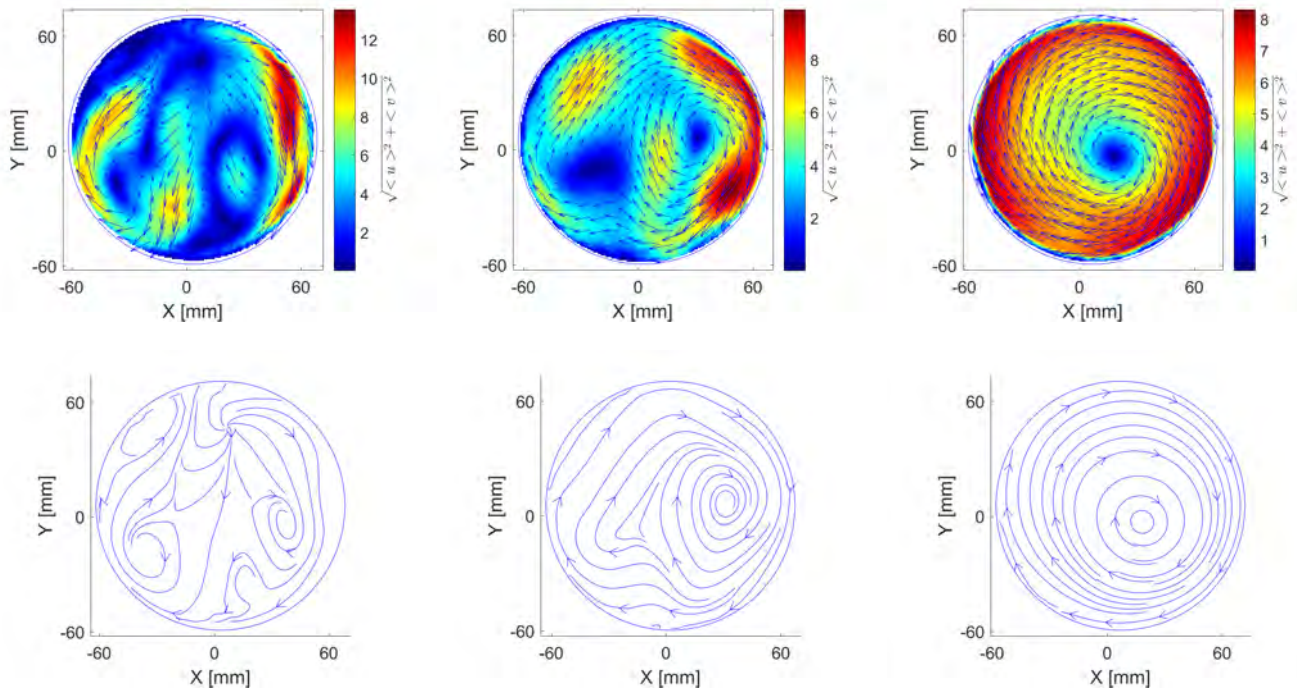


Figure 5: From left to right: 42 mm, 100 mm and 228 mm. From top to bottom: mean velocity field and streamlines. Valve lift: 15 mm.

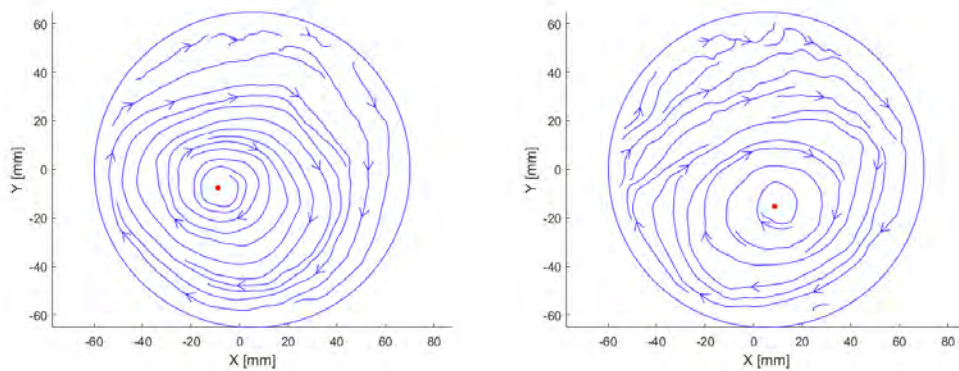


Figure 6: Instantaneous swirl centre position for two different snapshots of the 350 mm measurement plane, with 15 mm valve lift. The swirl centre position is indicated by the red dot.

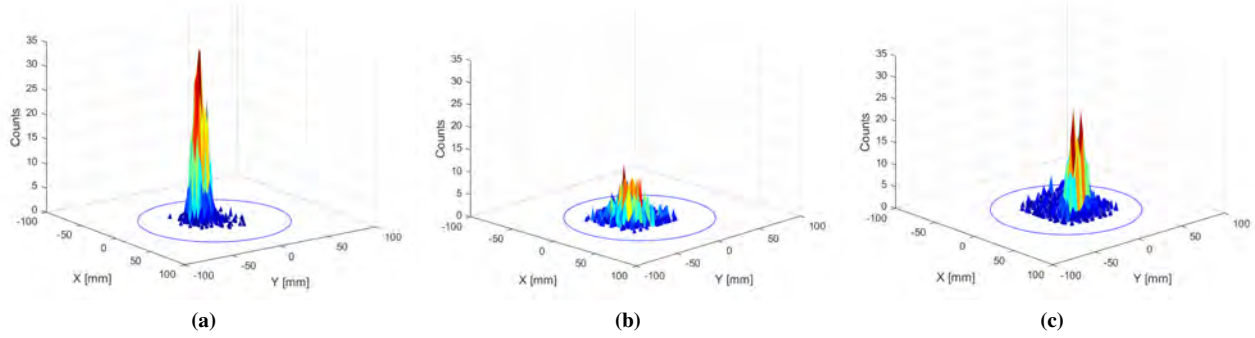


Figure 7: Swirl centre distribution for different cases: 350 mm measurement plane, 15 mm valve lift (a) and 10 mm valve lift (b); 170 mm measurement plane, 15 mm valve lift (c).

planes, 170 mm and 350 mm, and two different valve lifts for the 350 mm plane, have been studied. Indeed, the 350 mm measurement plane, with 15 mm valve lift (Figure 7(a)) presents a higher and more concentrated centre distribution compared to the same plane, with 10 mm valve lift (Figure 7(b)) and to the 170 mm plane, with 15 mm valve lift (Figure 7(c)), as expected.

V.C. POD analysis

Performing the POD analysis, comparing the first mode of uv covariance with the corresponding mean velocity field they present the same flow behaviour. As example, in Figure 8, the 80 mm measurement plane is presented. This can be explained recalling that the POD decomposes the studied flow field into different basis modes, each of them representing several flow structures, with associated energy levels. Organizing the modes in a decreasing energy content, it is possible to compare the energy contained in the first mode with the energy associated to the other modes. Analysing the first mode of 350 mm and 80 mm measurement planes in Figure 9, it can be noticed that the first mode has the most part of the total energy content. Indeed, for the 350 mm plane the energy contained in the first mode is 87%, compared to less than 1% starting from the second mode; for the 80 mm plane, the energy associated to the first mode is 25%, while the second mode contains 2%. This is why the first mode of uv covariance is very similar to the corresponding mean velocity field.

The energy content in the first mode of 350 mm is considerably higher compared to the equivalent mode of the 80 mm plane. Since the first plane presents a more organized flow structure, it is supposed that there could be a tendency to an increase in the first mode energy content going from the top to the bottom of the cylinder. Then, the first mode energy content is determined for each measurement plane and it is reported in Figure 10(a). In particular, a general tendency in an increase in the energy content can be appreciated. However, for the 60 mm, 80 mm and 140 mm planes, the energy level is less than expected. A possible explanation can be found looking to the mean velocity field. In Table 2 is reported the maximum velocity magnitude value for each of these planes. It can be noticed that 60 mm and 80 mm planes have a maximum velocity magnitude smaller than the 42 mm plane. The same can be seen comparing the 140 mm plane with 120 mm plane.

Measurement Plane [mm]	42	60	80	120	140
Max. Vel. Magn. [m/s]	$\simeq 13$	$\simeq 11$	$\simeq 11$	$\simeq 11$	$\simeq 10$

Table 2: Maximum velocity magnitude at different measurement planes, for mono configuration setup.

Finally, in Figure 10(b), it is possible to see how the total kinetic energy content changes along the cylinder axis. In particular, a decrease between measurement planes 42 mm and 60 mm can be appreciated. Going further down along the cylinder axis, the total kinetic energy content is generally constant, meaning that there is no dissipation of the swirl motion.

V.D. Mean velocity in Tumble plane

One significant tumble plane, related to tumble plane 1 region, is reported. The measurements related to tumble plane 2 region are mainly used for the 3D3C reconstruction.

To clearly understand the analysed region, the positive direction of rotation of the measurement plane and the valve positions are shown in Figure 4(b).

In Figure 11 the W velocity component and streamlines, referred to the mean velocity field, corresponding to 60° is reported. Looking at the streamlines, the presence of a recirculation bubble, the tumble motion, is evident, where

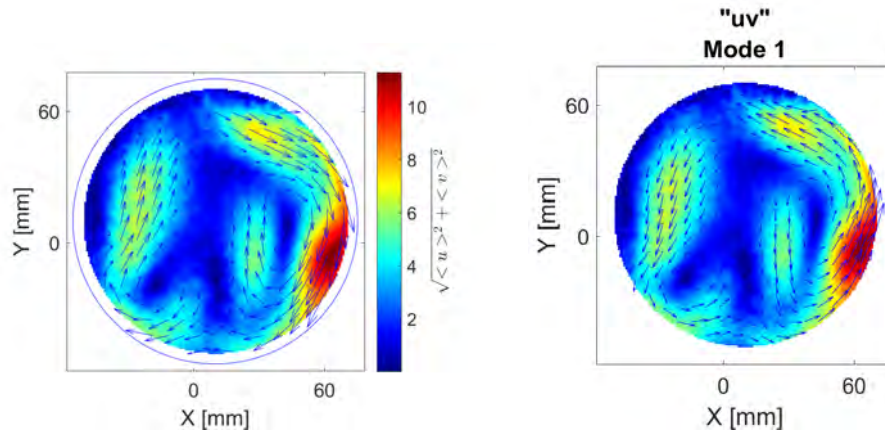


Figure 8: From left to right, comparison between mean velocity field of 80 mm measurement plane, 15 mm valve lift, and first mode of uv covariance, obtained trough POD analysis.

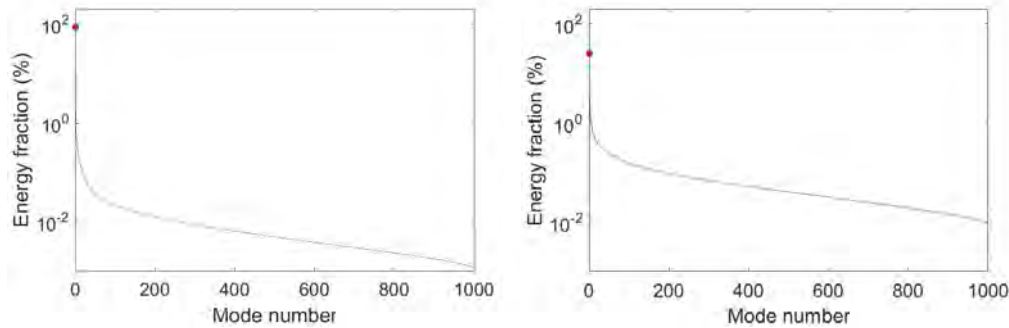


Figure 9: From left to right: mode energy variation for 350 mm measurement plane and for 80 mm measurement plane, both with 15 mm valve lift. The red dot indicates the energy content of Mode 1.

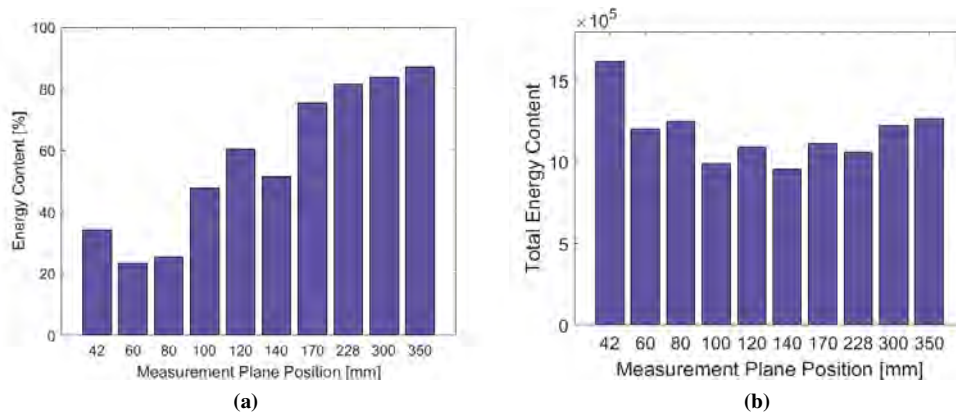


Figure 10: (a) Kinetic energy content variation along the cylinder axis, associated to Mode 1; (b) total kinetic energy variation along the cylinder axis.

a jet coming from the valves is observable. Indeed, on the left side of the related figure high velocity fluid is moving downwards, while on the right side, of the same figure, the velocity is directed in the opposite direction.

V.E. 3D3C Reconstruction

By means of all measurement planes obtained from the stereo PIV configuration, it has been possible to reconstruct the flow field in the entire cylinder volume.

In Figure 12 (a) and (b), streamtubes obtained from the 3D3C reconstruction are reported. In particular, it is possible to appreciate both tumble and swirl motions. The first can be recognised in the left picture, where the presence of a strong recirculation bubble, below the valve region is confirmed. While, the swirl can be distinguished in the right picture, where

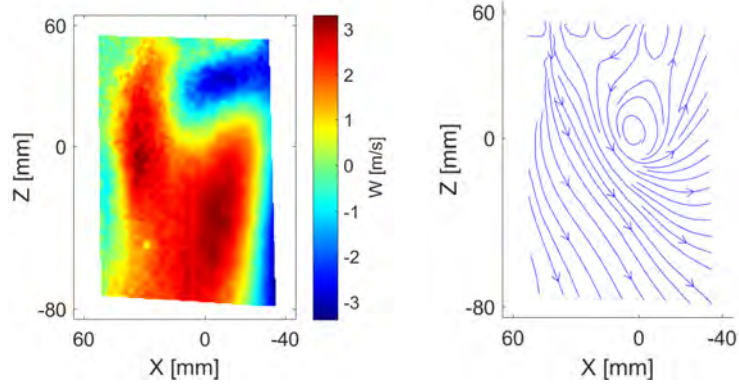


Figure 11: From left to right: W velocity component, streamlines of the mean velocity field. At 60° measurement plane, with a valve lift of 15 mm.

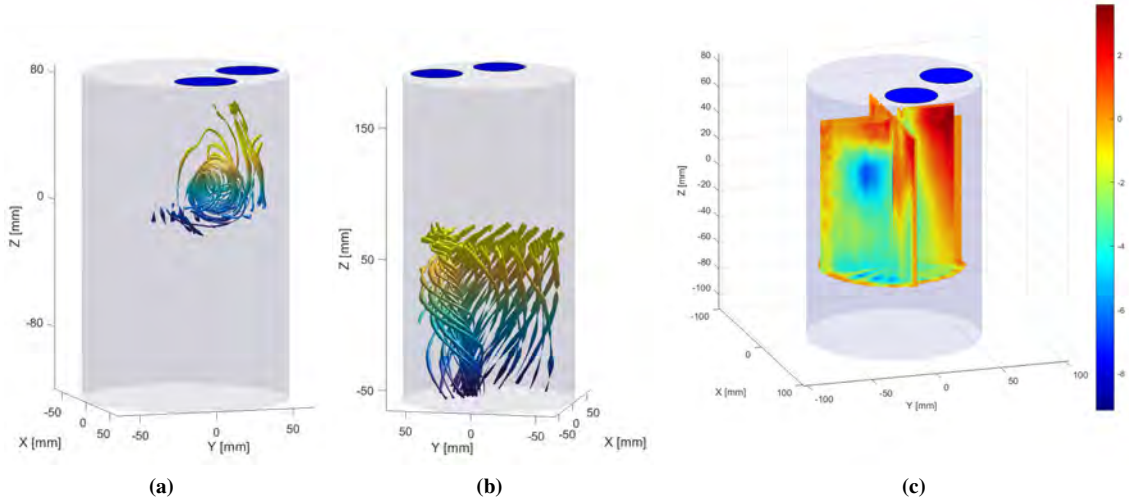


Figure 12: (a), (b) Streamtubes obtained from the 3D3C reconstruction, with a valve lift of 15 mm. The colour indicates the Z position; the width of tubes is proportional to the local value of the divergence. (a) Tumble plane 1; (b) tumble plane 2. (c) 3D3C flow visualization. Colour indicates W velocity component. Positive direction of velocity is downwards.

it is confirmed the existence of a dominant vortex in Region 3, as reported in Section (V.A).

In Figure 12(c), a 3D3C visualization of the flow of tumble plane 1, for the region below the valves, is shown. In particular, the colour indicates the W velocity component, directed along the cylinder axis. The picture is useful to visualize the dominant presence of the jets near the valves. Successively, the flow collides near the cylinder wall opposite to the valves, to finally dive down into the lower region.

V.F. Comparison with LES simulations

The mono PIV swirl results are compared with some significant measurement planes obtained from LES simulations, performed in Scania. In particular, in Figure 13 the 80 mm and 170 mm measurement planes are reported. It is possible to notice that the main structures, such as the vortex core for planes positioned far downstream, can be identified in the same positions. Moreover, in order to have an accurate comparison, the magnitude of the in-plane velocity is scaled with the corresponding mean velocity. A general correspondence of the order of magnitude for these quantities can be observed.

For the reasons mentioned above, it is possible to conclude that the LES simulations are able to capture the main flow characteristics with good accuracy.

VI. Conclusion

In this work, performed at Scania CV AB, the main structures of swirl and tumble motions are investigated, focusing on the intake stroke phase of a Diesel engine. The cylinder head is tested in several flow conditions, by means of Particle

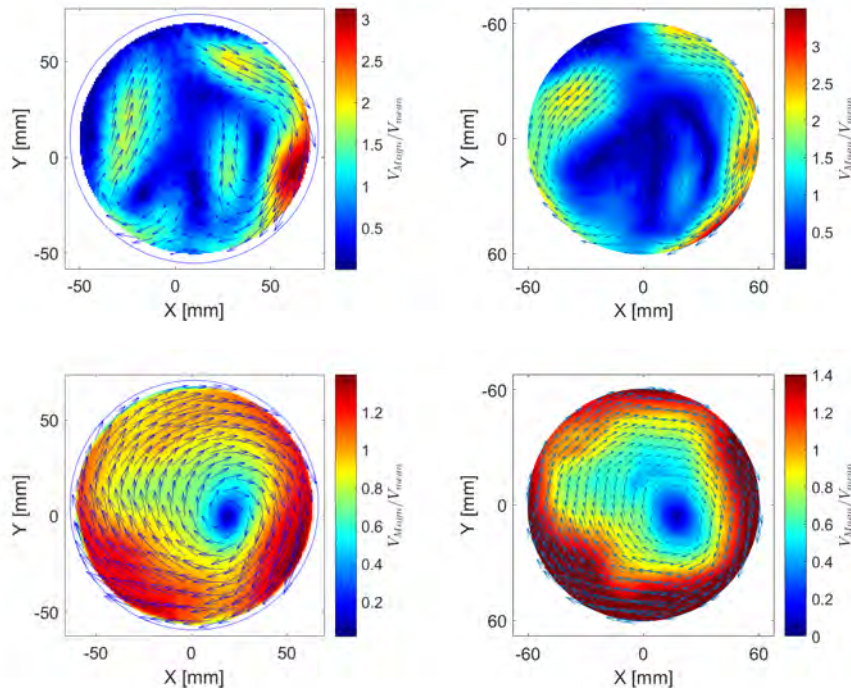


Figure 13: Comparison between mono PIV results and LES simulations. From left to right: mono PIV results, LES simulations. From top to bottom: 80 mm, 170 mm measurement planes. Point of view from the bottom. Valve position as indicated in Figure 4.

Image Velocimetry.

Analysing the swirling motion along the cylinder axis, it is possible to identify three main regions. Moreover, the organization of the swirl structure is studied by means of instantaneous swirl centre detection. Finally, by means of a POD analysis, the kinetic energy content in the different modes is analysed.

Studying the tumble motion, two main characteristics are observed: the presence of a recirculation bubble and a strong jet coming from the valves. In addition, the measurements obtained using a stereoscopic configuration, allow to study the flow field in the entire cylinder volume, performing a three-dimensional three-component (3D3C) reconstruction.

Finally, the mono PIV results are compared with LES simulations. Then, it is possible to conclude that the simulations are valid, since they are able to capture the main flow characteristics with a considerable accuracy.

All the measurements are performed without a piston and keeping the valve lift fixed. The effect of a moving piston, with moving valves is currently object of a joint project between Scania CV AB and KTH Mechanics department.

References

- [1] Lumley, J. L., (1999), *Engines: An Introduction*, Cambridge University Press, Cambridge, UK.
- [2] Buljak, V., (2011), *Inverse Analyses with Model Reduction*, Springer-Verlag, Heidelberg, Germany.
- [3] Chen, H., Reuss, D. L., Hung, D. L. S., Sick, V., *A practical guide for using proper orthogonal decomposition in engine research*, International Journal of Engine Research.
- [4] Raffel, M., Willert, C., Wereley, S., Kompenhans, J., (2007), *Particle Image Velocimetry A Practical Guide (Second ed., Experimental Fluid Mechanics)*, Springer-Verlag, Heidelberg, Germany.
- [5] LaVision GmbH, (2010), *Flow Master, product manual*, Göttingen, Germany.
- [6] Boutier, A. (2013), *Laser Velocimetry in Fluid Mechanics*, ISTE Ltd, London, UK.
- [7] Merklinger, H. M., (1996), *Focusing the View Camera*, Dartmouth, Nova Scotia.
- [8] Jiang, M., Machiraju, R., Thompson, D. (2004), *Detection and Visualization of Vortices*, Visualization Handbook, Chapter 14, pp.295, XXVII-309, XXVIII.
- [9] Fahringer, T. W., Thurow, B. S., (2012), *Tomographic Reconstruction of a 3-D Flow Field Using a Plenoptic Camera*, Auburn University, USA.
- [10] Chen, H., Sick, V., (2017), *Three-Dimensional Three-Component Air Flow Visualization in a Steady-State Engine Flow Bench Using a Plenoptic Camera*, SAE Int. J. Engines 10(2):625-635, doi:10.4271/2017-01-0614.
- [11] Rabault, J., (2015), *PIV Investigation of the Intake Flow in a Parallel Valves Diesel Engine Cylinder*, Master Thesis, KTH Mechanics, Stockholm, Sweden.
- [12] Vernet, J., (2012), *Detailed study of steady in-cylinder flow and turbulence using stereoPIV*, Master Thesis, KTH Mechanics, Stockholm, Sweden.